Choriocapillaris and Retinal Vascular Alterations in Presymptomatic Alzheimer's Disease

Giulia Corradetti,[1,2] Deniz Oncel,[1] Shin Kadomoto,[1] Xianghong Arakaki,[3] Robert A. Kloner,[4–6] Alfredo A. Sadun,[1,2] SriniVas R. Sadda,[1,2] and Jane W. Chan[1,2]

[1]Doheny Eye Institute, Pasadena, California, United States
[2]Department of Ophthalmology David Geffen School of Medicine, University of California Los Angeles, Los Angeles, California, United States
[3]Cognition and Brain Integration Laboratory, Department of Neurosciences, Huntington Medical Research Institutes, Pasadena, California, United States
[4]Clinical Neuroscience, Department of Neurosciences, Huntington Medical Research Institutes, Pasadena, California, United States
[5]Cardiovascular Research Institute, Huntington Medical Research Institutes, Pasadena, California, United States
[6]Cardiovascular Division, Department of Medicine Keck School of Medicine of University of Southern California, Los Angeles, California, United States

Correspondence: Jane W. Chan, Doheny Eye Institute, 625 South Fair Oaks Avenue, Suite 227, Pasadena, CA 91105, USA; janechan098@gmail.com.

Received: July 15, 2023
Accepted: January 8, 2024
Published: January 31, 2024

Citation: Corradetti G, Oncel D, Kadomoto S, et al. Choriocapillaris and retinal vascular alterations in presymptomatic Alzheimer's disease. *Invest Ophthalmol Vis Sci.* 2024;65(1):47. https://doi.org/10.1167/iovs.65.1.47

Purpose. To compare optical coherence tomography angiography (OCTA) retina metrics between cognitively healthy subjects with pathological versus normal cerebrospinal fluid (CSF) Aβ_{42}/tau ratios.

Methods. Swept-source OCTA scans were collected using the Zeiss PLEX Elite 9000 and analyzed on 23 cognitively healthy (CH) subjects who had previously undergone CSF analysis. Thirteen subjects had a pathological Aβ_{42}/tau (PAT) ratio of <2.7132, indicative of presymptomatic Alzheimer's disease (AD), and 10 had a normal Aβ_{42}/tau (NAT) ratio of ≥2.7132. OCTA en face images of the superficial vascular complex (SVC) and deep vascular complex were binarized and skeletonized to quantify the perfusion density (PD), vessel length density (VLD), and fractal dimension (FrD). The foveal avascular zone (FAZ) area was calculated using the SVC slab. Choriocapillaris flow deficits (CCFDs) were computed from the en face OCTA slab of the CC. The above parameters were compared between CH-PATs and CH-NATs.

Results. Compared to CH-NATs, CH-PATs showed significantly decreased PD, VLD, and FrD in the SVC, with a significantly increased FAZ area and CCFDs.

Conclusions. Swept-source OCTA analysis of the SVC and CC suggests a significant vascular loss at the CH stage of pre-AD that might be an indicator of a neurodegenerative process initiated by the impaired clearance of Aβ_{42} in the blood vessel wall and by phosphorylated tau accumulation in the perivascular spaces, a process that most likely mirrors that in the brain. If confirmed in larger longitudinal studies, OCTA retinal and inner choroidal metrics may be important biomarkers for assessing presymptomatic AD.

Keywords: optical coherence tomography angiography, Alzheimer's disease, imaging biomarkers, amyloid proteins, neurodegenerative disorders

As the aging population expands globally, Alzheimer's disease (AD) has become the most common neurodegenerative disorder causing progressive cognitive impairment. It is estimated that AD will affect over 153 million people by 2050, with physical, psychological, social, and economic implications, especially in low and middle-income countries.[1] The normal aging process and AD pathology are thought to interact to accelerate the neurodegenerative process.

Compared to magnetic resonance imaging and positron emission tomography (PET) imaging, an increasing level of serum phosphorylated tau (p-tau181 and p-tau127)[2] and a decreasing cerebrospinal fluid (CSF) A$\beta_{42/40}$ ratio can quantitatively better define the progression from preclinical AD to manifest AD.[3]

The AD pathology in the retinal vasculature and the retinal layers has been found to mirror that in the brain and has provided the basis for in vivo optical coherence tomography angiography (OCTA) to capture the disease process in greater detail in real time. Aβ_{40} accumulation has been shown inside and around all layers of the blood vessels in the brain and retina, as shown in postmortem brain and eye tissues from patients with mild cognitive impairment (MCI) and AD. These retinal vascular Aβ_{40} deposits have been correlated with the beta-amyloid plaque load in the entorhinal cortex that is predictive of cognitive decline.[4]

In postmortem eye tissues from patients with MCI and AD, the blood–retinal barrier (BRB) is compromised by a vasculopathy in which retinal pericytes undergo apoptosis with progressive Aβ_{40} and Aβ_{42} accumulation. The levels of platelet-derived growth factor receptor β (PDGFRβ) associated with the blood–brain barrier serve as a pericyte injury biomarker in the CSF. These levels have been shown to be correlated with cognitive decline in apolipoprotein E (ApoE4) carriers after accounting for Aβ_{42} and tau status.[5,6] Based on these histopathological studies in human eyes with AD, we hypothesized that the microvasculature changes in the retina and choroid might precede cognitive impairment in preclinical AD. We compared the swept-source OCTA (SS-OCTA) metrics in cognitively normal subjects with normal and pathological CSF Aβ_{42}/tau ratios.

Methods

This prospective cross-sectional observational study was approved by the Institutional Review Boards (IRBs) of the University of California Los Angeles (#15-000083) and the Huntington Medical Research Institutes (#33797). Informed consent was provided by each study subject. The research adhered to the tenets of the Declaration of Helsinki and the regulations of the Health Insurance Portability and Accountability Act.

Participants

Participants over 60 years of age without cognitive impairment, recruited at the Huntington Medical Research Institutes (Pasadena, CA, USA) for cognitive aging research and tested for CSF Alzheimer's biomarkers, were considered eligible for this prospective cross-sectional observational study. Two groups were defined based on the CSF Aβ_{42}/tau cutoff ratio of 2.7132, which has been reported to classify more than 85% of probable preclinical AD among cognitively healthy (CH) individuals: CH participants with pathological Aβ_{42}/tau ratios of $<$ 2.7132 (CH-PATs) and CH participants with normal Aβ_{42}/tau protein ratios of $\geq$2.7132 (CH-NATs).[7] In this study, CH-PAT individuals were considered as having preclinical AD. Each of our study participants underwent a series of neuropsychological tests, including the Functional Activity Questionnaire,[8] Mini-Mental State Exam (MMSE)-7 and MMSE-World,[9] Montreal Cognitive Assessment,[10] Geriatric Depression Scale,[11] Clin-

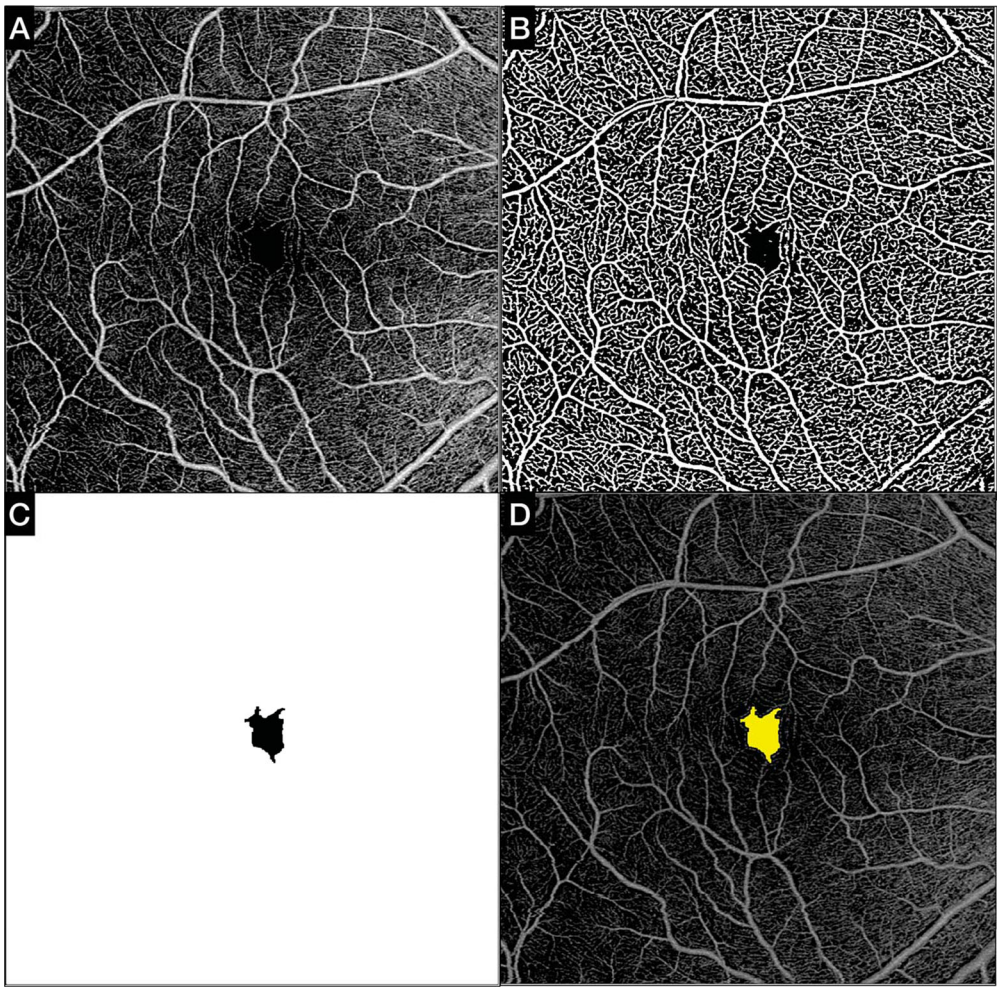

Figure 1. Automated quantitative analysis of the FAZ (mm^2). (**A**) The FAZ area was computed using the default SVC OCTA en face slab and a swept-source device. (**B**) A filter was applied to the default SVC slab, and subsequently an auto threshold algorithm was computed to binarize the image. (**C**) The algorithm automatically detected the foveal areas without vascularity (FAZ) and generated a mask. (**D**) The FAZ map created by the software in **C** corresponds with the FAZ on the SVC slab.

Investigative Ophthalmology & Visual Science

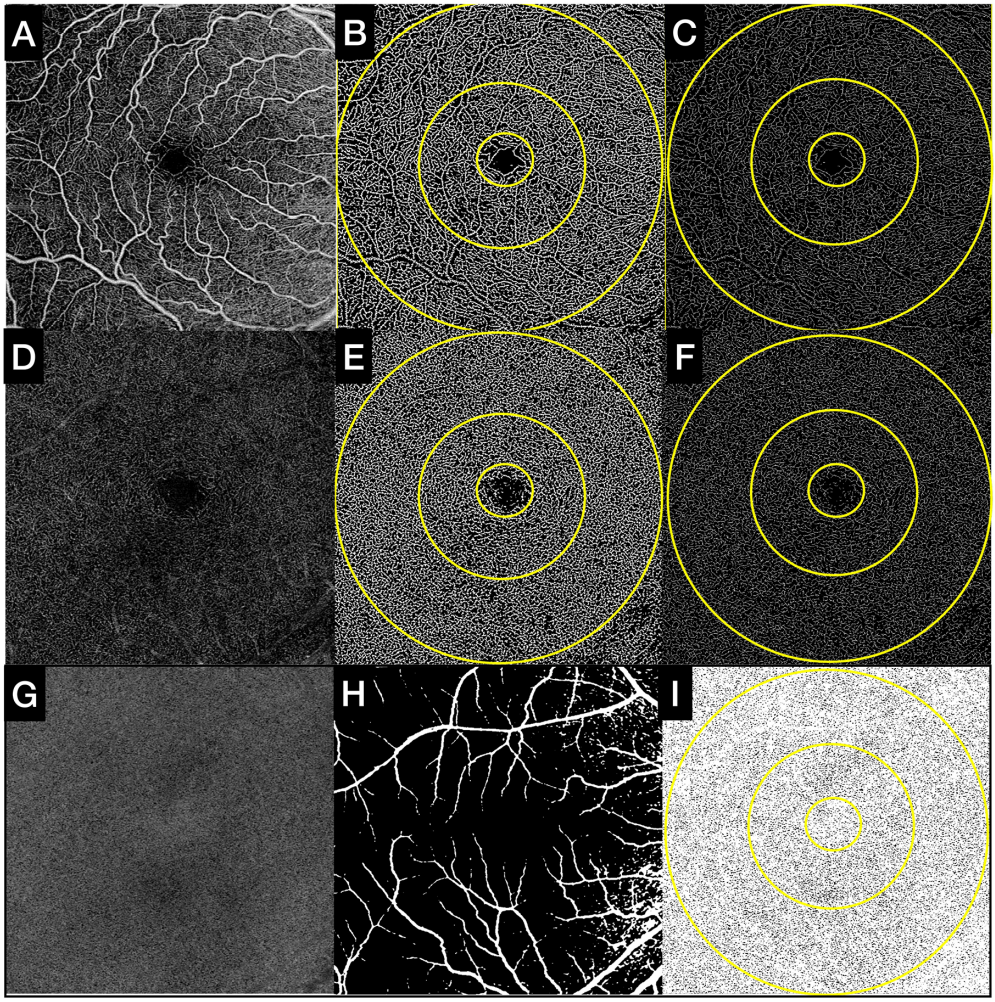

Figure 2. Quantitative analysis of SVC, DVC, and CC in subjects without cognitive impairment. (*Upper row*, **A–C**) (**A**) Default SVC OCTA en face slab as exported from the OCTA device (6 × 6 mm; 1024 × 1024 pixels). (**B**) Binarized SVC OCTA en face slab used to compute the PD assessment. (**C**) Skeletonized SVC OCTA en face slab used to compute the VLD assessment. (*Middle row*, **D–F**) (**D**) Default DVC OCTA en face slab as exported from the OCTA device (6 × 6 mm; 1024 × 1024 pixels). (**E**) Binarized DVC OCTA en face slab used to compute the PD assessment. (**F**) Skeletonized DVC OCTA en face slab used to compute the VLD assessment. (*Lower row*, **G–I**) (**G**) Custom 16-µm-thick CC OCTA en face slab positioned 4 µm below BM. (**H**) Superficial mask that was overlapped to the CC slab; large and superficial vessels were eliminated from the computation of CC flow deficits. (**I**) CC OCTA en face slab binarized with superficial mask overlapped was used to quantify the CC flow deficits. All measurements were computed in the slab and the 3-mm and 6-mm ETDRS rings, as shown by the overlapped rings in **B**, **C**, **E**, **F**, and **I**.

ical Dementia Rating (CDR) scale,[12] and Clinical Dementia Rating Sum of Boxes.[13] Biofluid collection and retinal imaging were performed within 1 year in 92% of the total study subjects, and the remainder within 2 years.

Exclusion criteria included the following: images with signal strength <7, as per device output; images with large shadowing, decentration, motion artifacts, and additional noise that could impair the quantitative analysis; any previous treatment in the study eye, including vitreoretinal surgery, laser photocoagulation, anti-vascular endothelial growth factor injections, and photodynamic therapy; history of ocular inflammation in the study eye; or any preexisting retinal and choroidal diseases, as determined by structural OCT and SS-OCTA. Only one eye per patient was included in the study, and, when both eyes were eligible for the analysis, the eye with the image of the highest quality was chosen as the study eye. Only those individuals who had no or only one of the vascular risk factors (cardiovascular disease, hypertension, hyperlipidemia, type 2 diabetes, atrial fibrillation, or transient ischemic attack) qualified for study entry. Less than 1% of the participants had only one of the vascular risk factors. It has been shown that having a single vascular risk factor is common and not necessarily associated with increased cerebrovascular disease in older adults with AD. An increased burden of vascular risk factors was defined as an individual having two or more of them.[14,15]

OCTA Imaging

OCTA 6 × 6-mm images centered on the fovea (512 A-scans × 512 B-scans) from all CH subjects (CH-PATs and CH-NATs) were acquired on the PLEX Elite 9000 (Carl Zeiss Meditec, Jena, Germany) and were reviewed for quality. The PLEX Elite 9000 device has a swept light source with a central wavelength of 1050 nm, a bandwidth of 100 nm, and an axial resolution in the tissue of ~5 µm with a transverse resolution

at the retinal surface of ~20 µm. The device operates at an A-scan rate of 100,000 A-scans per second and utilizes an ultrahigh-sensitive optical microangiography algorithm.[16]

For each OCTA 6 × 6-mm volume, the inner retinal vascular networks (superficial and deep vascular complexes), the foveal avascular zone (FAZ), and the choriocapillaris (CC) were evaluated. The manufacturer's default segmentation boundaries were used for the superficial vascular complex (SVC) and deep vascular complex (DVC). The CC was defined as a custom 16-µm thick slab, with an inner boundary located 4 µm below Bruch's membrane (BM), which was generated using the manufacturer's proprietary BM segmentation algorithm (Carl Zeiss Meditec).[17] The manufacturer's automated projection artifact removal algorithm was applied. Images were inspected for segmentation errors, and manual adjustments were performed if required; thus, en face images of the SVC, DVC, and CC were exported for further analyses.

OCTA Quantitative Analyses

Quantitative analyses of all OCTA images were performed by investigators blinded to participant grouping (CH-PAT vs. CH-NAT). Perfusion density (PD) and vessel length density (VLD) were measured in both the SVC and DVC en face OCTA binarized and skeletonized images, respectively. The PD represents the percentage of vessel area with blood flow over the total area of the binarized image. The VLD is defined as the vessel length per unit area and was calculated on the skeletonized image.[18–21] Given that several studies have shown that the deep FAZ has less well-defined borders than the superficial FAZ,[22,23] we computed the FAZ area (in mm^2) using the binarized superficial en face OCTA slab only[22,23] (Fig. 1). The fractal dimension (FrD) provides information regarding the complexity of the vascular network by quantifying the degree of branching within the vasculature and was calculated on both SVC and DVC en face OCTA images.[24]

The CC en face OCTA slab was used to compute the CC flow deficit percentage (FD%). The en face CC OCTA slab was binarized using Phansalkar's local thresholding method (radius ~20 µm), and flow deficits with diameter <24 µm were excluded from the computation, as they were considered physiological intercapillary spacing. Large and superficial vessels were excluded from the computation.[25,26] All of the quantitative measurements were performed using an external software widely used for quantitative computation on ophthalmic digital images, ImageJ 1.50 (National Institutes of Health, Bethesda, MD, USA).

Superficial and deep PD, VLD, and CC FD% were computed within the 6 × 6-mm slab, an inner 3-mm Early Treatment of Diabetic Retinopathy Study (ETDRS) ring, and an outer 6-mm ETDRS ring. The inner 3-mm ETDRS ring was a 1000-µm-thick ring (diameter, 3 mm), defined by an inner and outer boundary at ~500 µm and 1500 µm from the foveal center. The outer 6-mm ETDRS ring was a 1500-µm-thick ring (diameter, 6 mm), defined by an inner boundary located ~1500 µm from the foveal center (Fig. 2).

Statistical Analyses

Statistical analysis was performed using SPSS Statistics 29 for Macintosh (IBM, Chicago, IL, USA). Quantitative variables were reported using means with standard deviations. The subjects were divided into two groups based on the $A\beta_{42}$/tau protein ratio: <2.7132 for CH-PATs and >2.7132 for CH-NATs. The samples were assessed for normal distribution using the Shapiro–Wilk test and were found to be normally distributed. The quantitative variables between the two groups were compared using an independent samples *t*-test when the equal variances assumption was met ($P > 0.05$, Levene's test) or Welch's test when the assumption of equal variances was violated. $P < 0.05$ was considered statistically significant for all tests.

Results

A total of 23 eyes from 23 subjects were included in the analysis. Thirteen subjects (56.5%) had a CSF $A\beta_{42}$/tau ratio < 2.7132 and were included in the CH-PAT group; 10 subjects were included in the CH-NAT group based on a CSF $A\beta_{42}$/tau ratio > 2.7132. The percentage of females in the CH-PAT group was 53.8% versus 70% in the CH-NAT group. The mean age was 82.2 ± 6.6 years in the CH-PAT group compared to 74.3 ± 11.7 years in the CH-NAT group ($P = 0.07$). Most of the enrolled subjects had ApoE genotypes that were low-risk for AD: 46.1% of the CH-PATs were ApoE genotype 3/3 versus 70% of the CH-NAT group; 23% of the CH-PATs had ApoE genotype 3/4 versus 20% of the CH-NATs; 7% of the CH-PAT group had ApoE genotype 4/4; and none of the CH-NATs had ApoE genotype 4/4.

None of the subjects in this analysis had a history or any evidence of neurological or other systemic diseases.

Table summarizes the results of the quantitative analyses from the SVC, DVC, and CC OCTA en face slabs derived from the entire scan area and within the 3-mm and 6-mm ETDRS rings. In summary, at the level of the SVC en face OCTA slabs, PD (%) and VLD (mm/mm^3) were significantly lower in the CH-PATs compared to the CH-NATs within the whole slab and the 6-mm (outer diameter) ETDRS ring (Fig. 3). The FAZ area was also significantly larger in CH-PAT eyes ($P = 0.02$). No statistically significant changes between

Table. Summary of OCTA Quantitative Analyses

	Mean (SD)		
	CH-PATs ($n = 13$)	CH-NATs ($n = 10$)	*P*
SVC PD%			0.01
Whole	26.9 (2.76)	29.0 (0.89)	
3-mm	26.7 (3.29)	28.3 (1.68)	0.15
6-mm	27.3 (2.64)	29.6 (0.94)	0.01
SVC VLD (mm/mm^3)			
Whole	9.7 (0.95)	10.5 (0.33)	0.01
3-mm	9.2 (1.55)	10.1 (0.53)	0.07
6-mm	9.8 (0.93)	10.7 (0.35)	0.00*
SVC FrD	1.60 (0.03)	1.63 (0.00*)	0.02
DVC PD%			
Whole	30.1 (0.97)	30.5 (0.62)	0.33
3-mm	30.5 (2.14)	31.1 (1.21)	0.36
6-mm	30.6 (0.94)	30.9 (0.61)	0.35
DVC VLD (mm/mm^3)			
Whole	11.1 (0.49)	11.1 (0.42)	0.85
3-mm	11.1 (0.73)	11.2 (0.50)	0.74
6-mm	11.3 (0.43)	11.3 (0.40)	0.87
DVC FrD	1.6 (0.17)	1.6 (0.01)	0.78
CC FD%			
Whole	11.2 (6.99)	6.5 (0.97)	0.03
3-mm	12.6 (7.9)	7.7 (1.6)	0.05
6-mm	10.4 (5.9)	6.5 (1.0)	0.03
FAZ area (mm^2)	0.27 (0.06)	0.19 (0.08)	0.02

* Indicates a value < 0.001.

Investigative Ophthalmology & Visual Science

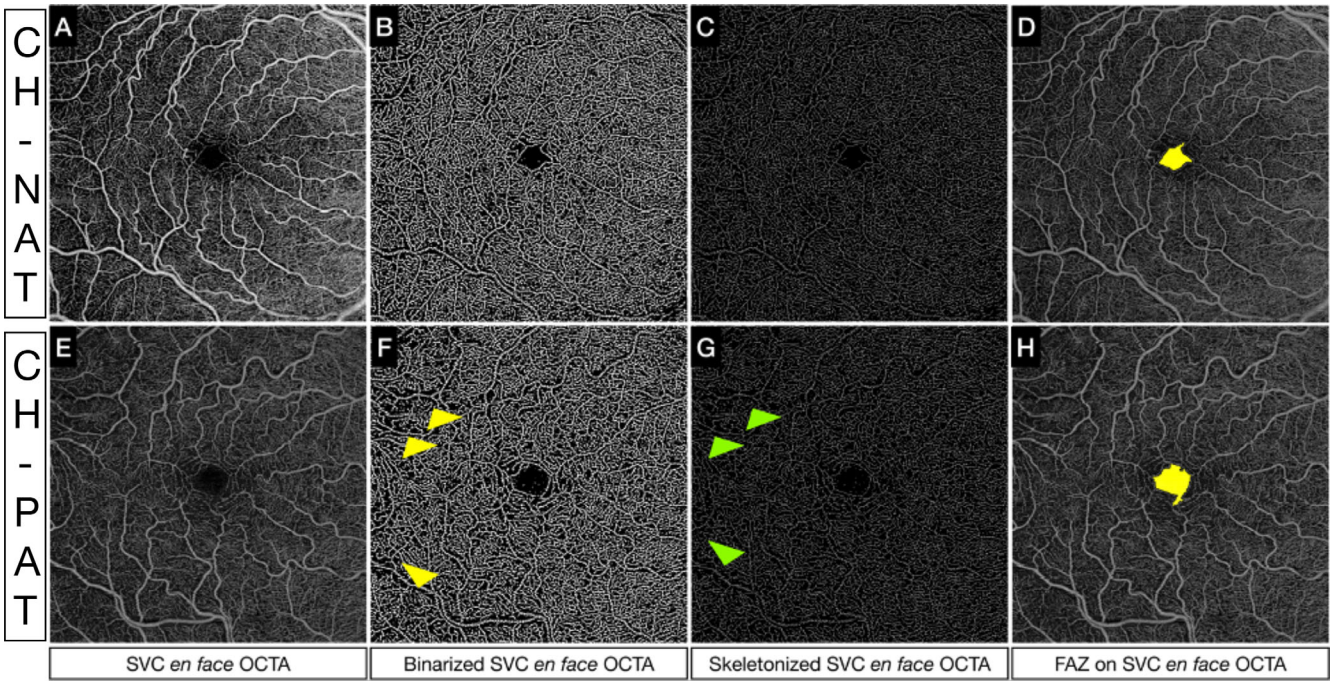

Figure 3. Quantitative analysis of SVC in a CH-PAT versus CH-NAT. (*Upper row*, **A–D**) (**A**) Superficial en face OCTA slab, (**B**) binarized superficial en face OCTA slab, (**C**) skeletonized superficial en face OCTA, and (**D**) segmented FAZ using a superficial en face OCTA slab in a CH-NAT subject. (Bottom row, **E–H**) (**E**) Superficial en face OCTA slab, (**F**) binarized superficial en face OCTA slab, (**G**) skeletonized superficial en face OCTA, and (**H**) segmented FAZ using a superficial en face OCTA slab in a CH-PAT subject. In **G** and **H**, we can appreciate the decreased PD (*yellow arrows*) and VLD (*green arrows*), respectively, in the outermost region of the OCTA slab from an eye of a CH-PAT subject.

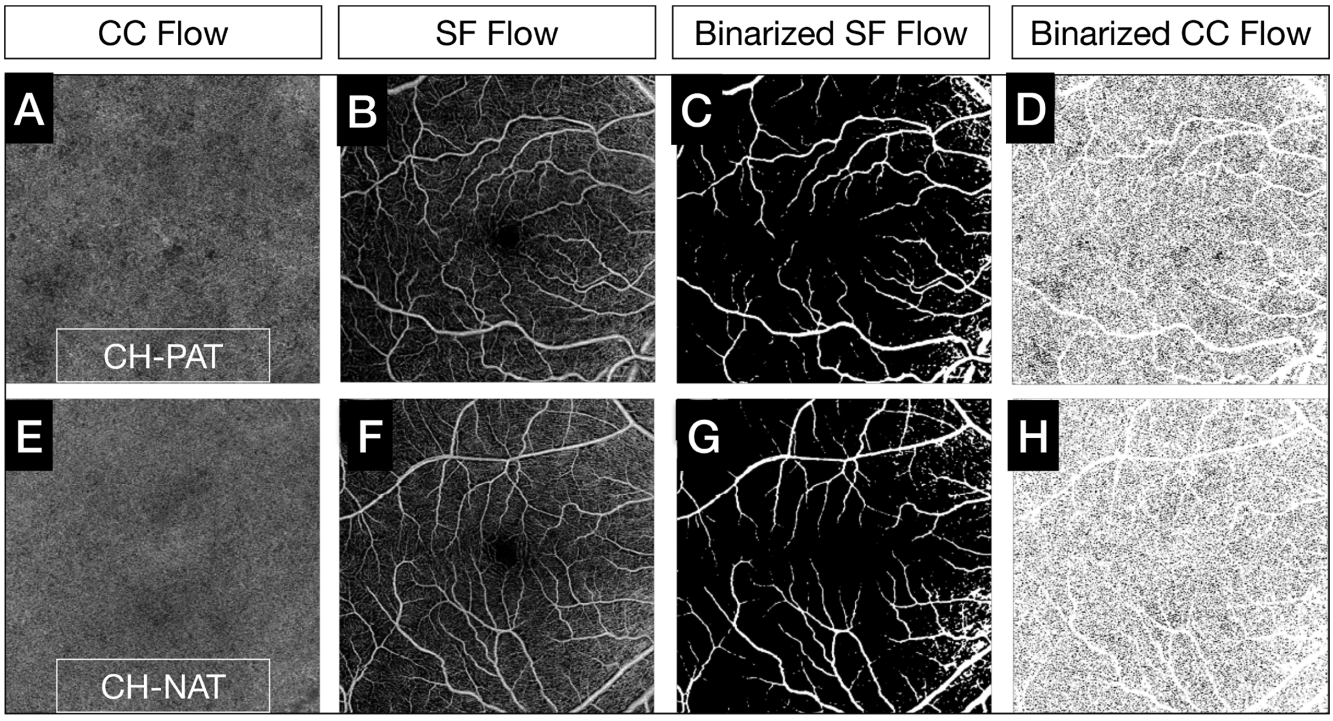

Figure 4. Comparison of CC flow deficits between CH-PAT and CH-NAT subjects. Customized CC en face OCTA slabs segmented just below BM (4–20 µm) were generated (**A**, **E**). The default superficial en face OCTA slabs (**B**, **F**) were binarized (**C**, **G**) and overlapped to the binarized CC en face OCTA slab to mask the projections of superficial and large vessels, which were excluded from the analyses. The final binarized CC en face OCTA slab used to compute the CC FD% is illustrated in **D** and **H**, and the CC en face OCTA slab from a CH-PAT eye shows increased CC FDs (**D**) compared to a CH-NAT eye (**H**).

Investigative Ophthalmology & Visual Science

the two groups were noted within the DCP at any level. CC FD% measurements within the whole 6 × 6-mm slab were significantly higher in the CH-PATs compared to the CH-NATs (Fig. 4). In the subanalysis, this relationship was confirmed, with the CH-PATs having greater CC FD% in both the 3-mm and 6-mm ETDRS rings compared to the CH-NATs.

Discussion

In this pilot study, we found that subjects with preclinical AD (CH-PATs) had significantly decreased PD and decreased VLD within the whole slab and the 6-mm ETDRS ring within the SVC, significant enlargement of the FAZ, and increased CC flow deficits compared to controls (CH-NATs), as shown in Table. The vessel architectural changes and perfusion abnormalities in our quantitative analysis of the inner retinal vasculature and CC provide in vivo evidence supporting a subclinical retinal and inner choroidal vasculopathy in the cognitively normal pre-AD stages.

Our study shows significantly increased CC FD% in the macular region of study subjects with a pathologic CSF Aβ_{42}/total tau ratio, a risk factor previously shown to predict progression to dementia.[27] Previously hypothesized mechanisms for choroidal and CC changes in AD include the pathological inflammatory cascades associated with progressive neurodegeneration and concomitant retinal/choroidal reduced blood flow in AD.[28,29] Pro-inflammatory molecules may drive the persistence of oxidative stress and lead to damage and dysfunction of the CC at earlier stages of the disease.[27,30,31] Damage of the CC can also lead to impaired blood flow and decreased oxygen delivery to the outer retina with subsequent photoreceptor dysfunction.[32]

Inner retinal capillary loss is represented by a significantly decreased PD, VLD, and FrD and an enlarged FAZ in the SVC. Cheung et al.[33] also described the microvascular retinal network as being more sparse in subjects with AD. These changes in the retinal vasculature may reflect similar changes in the cerebral microvasculature in the brain of patients affected by AD. Whether our preliminary OCTA abnormalities in the inner retinal layers correlate with the thinning of specific retinal layers will require further longitudinal analysis with OCT imaging. Our abnormal OCTA findings in the PATs group with increasing CSF levels of total tau relative to Aβ_{42} might support the two-hit vascular hypothesis of AD.[34] The first hit is from the loss of pericytes due to PDGFRβ deficiency causing vascular damage in the BRB, similar to that in the blood–brain barrier. The second hit is from the co-occurring Aβ and p-tau deposits that initiate and/or accelerate neuronal degeneration. The increased CSF levels of PDGFRβ have been shown to be correlated with cognitive decline in ApoE4 carriers, even after accounting for Aβ and tau levels.[5] Our findings of significant SVC alterations within the 6-mm (outer diameter) ETDRS ring and not within the 3-mm (inner diameter) ring support the hypothesis that AD pathology begins further in the retinal periphery and not from within the macula. Histopathologic findings have shown that the superior peripheral hemiretina is generally the most atrophic region.[35] A recent study also showed a higher Aβ_{42} density in the periphery versus the central retina in human donor eyes affected by MCI or AD.[36] The propensity of amyloid proteins to accumulate in peripheral areas of the retina implies that analyzing ultra-widefield topographic OCTA metrics in preclinical AD could provide valuable insights into the natural history of retinal amyloid pathology.

Our study results confirm some of the OCTA findings in two other studies also performed at the cognitively normal pre-AD stage. The increased FAZ area in the CH-PATs versus the CH-NATs was consistent with the enlarged FAZ in the study by O'Bryhim et al.[37,38] The authors defined pre-AD as having an elevated CSF Aβ_{42} level and/or a positive PET Aβ scan with a normal score on the CDR scale. OCTA was captured on an Optovue OCTA system (Visionix, Lombard, IL, USA) in a study cohort slightly younger than ours. After 3 years of follow-up, they found that their participants' FAZ and cognitive status did not change. It is also important to consider the wide variability in FAZ size among individuals of a similar age; thus, the FAZ area might not be the optimal biomarker for monitoring disease progression. Our finding of a significantly decreased SVC PD% and VLD (mm/mm^3) in the PATs versus NATs confirmed similar results from the second study by Ma et al.[39] Pre-AD was defined by the presence of an ApoE4 allele and normal cognitive status in a considerably larger cohort than ours. Although this study cohort was larger, the reliance on ApoE4 allele carriage and normal cognitive status for the definition of pre-AD does not align with the 2018 National Institute on Aging and Alzheimer's Association definition of AD.[40]

After 2 years of follow-up, no differences in the rate of change of the OCTA parameters obtained using the ZEISS AngioPlex system (Carl Zeiss Meditec) were detected between participants with the ApoE4 allele and those without. Compared to these two other studies, we used a swept-source device (PLEX Elite 9000), which allows for faster acquisition and deeper penetration to the choroid. We also analyzed our data using a widely validated algorithm to quantify the microvasculature from OCTA images.[17,41–43]

Our results differ from those reported by van de Kreeke et al.[44] Instead of a decrease in SVC PD% in the outer ETDRS ring and an increase in FAZ size in the pre-AD eyes versus the normal controls, the authors showed a significant increase in SVC vessel density percentage (VD%) in the inner ETDRS ring and no difference in the FAZ size in their cohort of PET Aβ-positives versus negatives. They hypothesized that hypoxia could have led to the compensatory recruitment of more capillaries filling up to increase the VD%. Measurements were performed on a ZEISS AngioPlex system in a slightly younger cohort than ours in which a positive PET Aβ scan defined pre-AD.

Our analysis of the above three publications regarding OCTA metrics in the cognitively normal pre-AD stages uncovered different pre-AD definitions that included relatively earlier or later stages of the prodrome period, measurements and analysis on various OCTA equipment, and different age ranges in each study cohort. These studies uncover some unmet clinical needs in current AD research: (1) a consensus for the inclusion and exclusion criteria of the preclinical AD stage; (2) a narrower age range of participants in the study cohort within 10 years because AD is an age-related disease; and (3) a consensus on OCTA methodology.

Our study was not without limitations. First, the sample size was small. The aim of this small prospective cross-sectional observational pilot study was to explore the capabilities of OCTA imaging in differentiating preclinical AD versus biological aging. The effect size between the CH-PATs and CH-NATs was small. Study recruitment of elderly individuals who had *no or only one* vascular risk factor was limited and contributed to our small sample size. Although this was important to determine the relationship between

Investigative Ophthalmology & Visual Science

pre-AD and the retinal and choroidal vasculature without the confounding effects of cardiovascular disease (CVD) and CVD risk factors, the exclusion of participants with CVD risk factors may limit the generalizability of the findings, given the high prevalence of comorbid CVD and CVD risk factors in the elderly. Our sample size was also limited because of the relatively invasive lumbar puncture procedure that discouraged some subjects to enroll.

Regarding study strengths, our study was conducted prospectively in a curated study cohort with the pre-AD stage quantitatively defined by CSF Aβ_{42}/total tau ratios. Most of our participants had low-risk AD genotypes (ApoE 3/3 alleles) and had retinal imaging done within 2 years of their CSF analysis. Our study cohort consisted of relatively older participants with a median age of about 80 years with no or only one vascular risk factor. Our SS-OCTA results distinguished the effects of aging in the NATs group from the effects of pre-AD with aging in the PATs group. This statistically significant difference was detectable because our study cohort was meticulously curated to include only individuals who had no or one vascular risk factor, as described in the Methods section.

In conclusion, our SS-OCTA measurements of the SVC and CC showed statistically significant abnormalities suggestive of attenuation of the superficial retinal and inner choroidal circulation in the earliest stages of pre-AD, as defined by an abnormal CSF Aβ/total tau ratio with normal cognition. Our study suggests that these retinal vascular abnormalities might serve as surrogate biomarkers of pre-AD. Because our OCTA findings demonstrated a statistically significant difference between the CH-PATs and the CH-NATs (normal aging group), the mild increased vascular damage in the CH-PATs is suggestive of the synergistic effect between beta-amyloid–dependent and beta-amyloid–independent pathways of normal aging in the progression of AD vasculopathy.[34] The biological plausibility and predictive value of our preliminary OCTA findings will have to be evaluated further in larger studies. It has been estimated that approximately 26% of probable preclinical AD progresses to symptomatic AD.[45]

Identifying early pathological biomarkers in preclinical AD is especially crucial for optimizing the design of clinical trials aimed at early interventions before irreversible cognitive impairment even begins. SS-OCTA is not yet widely available for clinical use, yet it allows for enhanced, high-resolution, high-definition, and more detailed visualization of the CC and retinal vascular complex, permitting more reliable quantitative analyses of OCTA metrics.

The variability in the quantitative analyses of OCTA metrics from different devices presents a challenge when comparing results across various studies. We think that the standardization of imaging methods and the pre-AD stage with serum biomarkers, such as p-tau217 and p-tau181,[46] would facilitate the identification of study subjects for recruitment into future pre-AD clinical trials.

Acknowledgments

The assistance in data collection provided by David Buennagel, BS, was greatly appreciated.

Supported by the Kuen Lau Research Foundation and a grant from the National Institute on Aging, National Institutes of Health (R01AG063857).

Disclosure: **G. Corradetti**, Nidek (L); **D. Oncel**, None; **S. Kadomoto**, Canon (C), Nidek (C); **X. Arakaki**, None; **R.A. Kloner**, None; **A.A. Sadun**, Chiesi (C), GenSight (C), Stealth (C); **S.R. Sadda**, 4DMT (C), Abbvie (C), Alexion (C), Allergan (C), Alnylam Pharmaceuticals (C), Amgen (C), Apellis Pharmaceuticals (C), Astellas (C), Bayer Healthcare Pharmaceuticals (C), Biogen (C), Boehringer Ingelheim (C), Carl Zeiss Meditec (C, L, S), Catalyst Pharmaceuticals (C), CenterVue (C), Genentech (C), Gyroscope Therapeutics (C), Heidelberg Engineering (C, L, S), Hoffmann-La Roche (C), Iveric Bio (C), Janssen Pharmaceuticals (C), Merck (C), Nanoscope (C), Nidek (L), Notal Vision (C), Novartis (C, L), Optos (C), Oxurion/Thrombogenics (C), Oyster Point Pharma (C), Pfizer (C), Regeneron Pharmaceuticals (C), Samsung Bioepis (C), Topcon Medical Systems (C, L), Vertex Pharmaceuticals (C); **J.W. Chan**, (C)

References

1. GBD 2019 Dementia Forecasting Collaborators. Estimation of the global prevalence of dementia in 2019 and forecasted prevalence in 2050: an analysis for the Global Burden of Disease Study 2019. *Lancet Public Health*. 2022;7(2):e105–e125.
2. Milà-Alomà M, Ashton NJ, Shekari M, et al. Plasma p-tau231 and p-tau217 as state markers of amyloid-β pathology in preclinical Alzheimer's disease. *Nat Med*. 2022;28(9):1797–1801.
3. Olsson B, Lautner R, Andreasson U, et al. CSF and blood biomarkers for the diagnosis of Alzheimer's disease: a systematic review and meta-analysis. *Lancet Neurol*. 2016;15(7):673–684.
4. Shi H, Koronyo Y, Rentsendorj A, et al. Retinal vasculopathy in Alzheimer's disease. *Front Neurosci*. 2021;15:731614.
5. Montagne A, Nation DA, Sagare AP, et al. APOE4 leads to blood–brain barrier dysfunction predicting cognitive decline. *Nature*. 2020;581(7806):71–76.
6. Fagan AM, Shaw LM, Xiong C, et al. Comparison of analytical platforms for cerebrospinal fluid measures of β-amyloid 1-42, total tau, and p-tau$_{181}$ for identifying Alzheimer disease amyloid plaque pathology. *Arch Neurol*. 2011;68(9):1137–1144.
7. Harrington MG, Chiang J, Pogoda JM, et al. Executive function changes before memory in preclinical Alzheimer's pathology: a prospective, cross-sectional, case control study. *PLoS One*. 2013;8(11):e79378.
8. Pfeffer RI, Kurosaki TT, Harrah CH, Jr, Chance JM, Filos S. Measurement of functional activities in older adults in the community. *J Gerontol*. 1982;37(3):323–329.
9. Crum RM, Anthony JC, Bassett SS, Folstein MF. Population-based norms for the Mini-Mental State Examination by age and educational level. *JAMA*. 1993;269(18):2386–2391.
10. Freitas S, Simões MR, Alves L, Santana I. Montreal cognitive assessment: validation study for mild cognitive impairment and Alzheimer disease. *Alzheimer Dis Assoc Disord*. 2013;27(1):37–43.
11. Yesavage JA. Geriatric Depression Scale. *Psychopharmacol Bull*. 1988;24(4):709–711.
12. Berg L. Clinical Dementia Rating (CDR). *Psychopharmacol Bull*. 1988;24(4):637–639.
13. Coley N, Andrieu S, Jaros M, Weiner M, Cedarbaum J, Vellas B. Suitability of the Clinical Dementia Rating-Sum of Boxes as a single primary endpoint for Alzheimer's disease trials. *Alzheimers Dement*. 2011;7(6):602–610.e2.
14. Nation DA, Delano-Wood L, Bangen KJ, et al. Antemortem pulse pressure elevation predicts cerebrovascular disease in autopsy-confirmed Alzheimer's disease. *J Alzheimers Dis*. 2012;30(3):595–603.
15. Bangen KJ, Nation DA, Delano-Wood L, et al. Aggregate effects of vascular risk factors on cerebrovascular changes in

autopsy-confirmed Alzheimer's disease. *Alzheimers Dement*. 2015;11(4):394–403.e1.
16. Wang RK, An L, Francis P, Wilson DJ. Depth-resolved imaging of capillary networks in retina and choroid using ultrahigh sensitive optical microangiography. *Opt Lett*. 2010;35(9):1467–1469.
17. Chu Z, Zhang Q, Gregori G, Rosenfeld PJ, Wang RK. Guidelines for imaging the choriocapillaris using OCT angiography. *Am J Ophthalmol*. 2021;222:92–101.
18. Smith CA, Josey VL, West ME, et al. Variability of scan quality and perfusion density in longitudinal optical coherence tomography angiography imaging [published online ahead of print October 19, 2023]. *Br J Ophthalmol*, https://doi.org/10.1136/bjo-2022-322979.
19. Stino H, de Llano Pato E, Steiner I, et al. Macular microvascular perfusion status in hypertensive patients with chronic kidney disease. *J Clin Med Res*. 2023;12(17):5493.
20. Śpiewak D, Witek K, Drzyzga Ł, Mrukwa-Kominek E. An analysis of optical coherence tomography angiography (OCT-A) perfusion density maps in patients treated for retinal vein occlusion with intravitreal aflibercept. *Diagnostics (Basel)*. 2023;13(19):3100.
21. Yospon T, Rojananuangnit K. Optical coherence tomography angiography (OCTA) differences in vessel perfusion density and flux index of the optic nerve and peri-papillary area in healthy, glaucoma suspect and glaucomatous eyes. *Clin Ophthalmol*. 2023;17:3011–3021.
22. Shiihara H, Terasaki H, Sonoda S, et al. Objective evaluation of size and shape of superficial foveal avascular zone in normal subjects by optical coherence tomography angiography. *Sci Rep*. 2018;8(1):10143.
23. Shiihara H, Sakamoto T, Yamashita T, et al. Reproducibility and differences in area of foveal avascular zone measured by three different optical coherence tomographic angiography instruments. *Sci Rep*. 2017;7(1):9853.
24. Yu Y, Zhang T, Meadway A, Wang X, Zhang Y. High-speed adaptive optics for imaging of the living human eye. *Opt Express*. 2015;23(18):23035–23052.
25. Zhang Q, Zheng F, Motulsky EH, et al. A novel strategy for quantifying choriocapillaris flow voids using swept-source OCT angiography. *Invest Ophthalmol Vis Sci*. 2018;59(1):203–211.
26. Zhang Q, Shi Y, Zhou H, et al. Accurate estimation of choriocapillaris flow deficits beyond normal intercapillary spacing with swept source OCT angiography. *Quant Imaging Med Surg*. 2018;8(7):658–666.
27. Asanad S, Ross-Cisneros FN, Barron E, et al. The retinal choroid as an oculovascular biomarker for Alzheimer's dementia: a histopathological study in severe disease. *Alzheimers Dement*. 2019;11:775–783.
28. Robbins CB, Grewal DS, Thompson AC, et al. Choroidal structural analysis in Alzheimer disease, mild cognitive impairment, and cognitively healthy controls. *Am J Ophthalmol*. 2021;223:359–367.
29. Marchesi VT. Alzheimer's dementia begins as a disease of small blood vessels, damaged by oxidative-induced inflammation and dysregulated amyloid metabolism: implications for early detection and therapy. *FASEB J*. 2011;25(1):5–13.
30. Bulut M, Kurtuluş F, Gözkaya O, et al. Evaluation of optical coherence tomography angiographic findings in Alzheimer's type dementia. *Br J Ophthalmol*. 2018;102(2):233–237.
31. Gharbiya M, Trebbastoni A, Parisi F, et al. Choroidal thinning as a new finding in Alzheimer's disease: evidence from enhanced depth imaging spectral domain optical coherence tomography. *J Alzheimers Dis*. 2014;40(4):907–917.
32. Tiosano L, Corradetti G, Sadda SR. Progression of choriocapillaris flow deficits in clinically stable intermediate age-related macular degeneration. *Eye (Lond)*. 2021;35(11):2991–2998.
33. Cheung CY-L, Ong YT, Ikram MK, et al. Microvascular network alterations in the retina of patients with Alzheimer's disease. *Alzheimers Dement*. 2014;10(2):135–142.
34. Zlokovic BV. Neurovascular pathways to neurodegeneration in Alzheimer's disease and other disorders. *Nat Rev Neurosci*. 2011;12(12):723–738.
35. Koronyo-Hamaoui M, Doustar J, Oviatt M, Black KL, Koronyo Y. Advances in retinal imaging: retinal amyloid imaging. In: Grzybowski A, Barboni P, eds. *OCT and Imaging in Central Nervous System Diseases: The Eye as a Window to the Brain*. Cham: Springer International Publishing; 2020:83–122.
36. Koronyo Y, Rentsendorj A, Mirzaei N, et al. Retinal pathological features and proteome signatures of Alzheimer's disease. *Acta Neuropathol*. 2023;145(4):409–438.
37. O'Bryhim BE, Apte RS, Kung N, Coble D, Van Stavern GP. Association of preclinical Alzheimer disease with optical coherence tomographic angiography findings. *JAMA Ophthalmol*. 2018;136(11):1242–1248.
38. O'Bryhim BE, Lin JB, Van Stavern GP, Apte RS. OCT angiography findings in preclinical Alzheimer's disease: 3-year follow-up. *Ophthalmology*. 2021;128(10):1489–1491.
39. Ma JP, Robbins CB, Lee JM, et al. Longitudinal analysis of the retina and choroid in cognitively normal individuals at higher genetic risk of Alzheimer disease. *Ophthalmol Retina*. 2022;6(7):607–619.
40. Jack CR, Jr, Bennett DA, Blennow K, et al. NIA-AA research framework: toward a biological definition of Alzheimer's disease. *Alzheimers Dement*. 2018;14(4):535–562.
41. Corvi F, Corradetti G, Sadda SR. Correlation between the angiographic choriocapillaris and the structural inner choroid. *Curr Eye Res*. 2021;46(6):871–877.
42. Corradetti G, Tiosano L, Nassisi M, et al. Scotopic microperimetric sensitivity and inner choroid flow deficits as predictors of progression to nascent geographic atrophy. *Br J Ophthalmol*. 2021;105(11):1584–1590.
43. Magesan K, Gnanaraj R, Tojjar J, et al. Fractal analysis of the macular region in healthy eyes using swept-source optical coherence tomography angiography. *Graefes Arch Clin Exp Ophthalmol*. 2023;261(10):2787–2794.
44. van de Kreeke JA, Nguyen H-T, Konijnenberg E, et al. Optical coherence tomography angiography in preclinical Alzheimer's disease. *Br J Ophthalmol*. 2020;104(2):157–161.
45. Vos SJ, Xiong C, Visser PJ, et al. Preclinical Alzheimer's disease and its outcome: a longitudinal cohort study. *Lancet Neurol*. 2013;12(10):957–965.
46. Therriault J, Servaes S, Tissot C, et al. Equivalence of plasma p-tau217 with cerebrospinal fluid in the diagnosis of Alzheimer's disease. *Alzheimers Dement*. 2023;19(11):4967–4977.

Investigative Ophthalmology & Visual Science